ADVANCED MATERIALS TECHNOLOGIES
www.advmattechnol.d

Scalable Processing Ultrathin Polymer Dielectric Films with a Generic Solution Based Approach for Wearable Soft Electronics

Sujie Chen, Sai Peng, Wenjian Sun, Guoying Gu, Qing Zhang, and Xiaojun Guo**

Wearable intelligence on human body requires light and soft electronics built on ultrathin supporting films. It would be ideal to have a generic and scalable approach for processing such ultrathin electronics based on various materials to accommodate different design requirements. In this work, a solution based delamination approach is developed using sodium hydroxide (NaOH) treated cross-linked polymethylmethacrylate (c-PMMA) film as the separation layer to process ultrathin polymer films. The c-PMMA layer has resistance to various solvents for coating different polymer materials on top. Reaction of the c-PMMA surface with mixture of NaOH and water reduces adhesion between the polymer film and the carrier substrate. The polymer film is thus able to be delaminated with facile processes. The approach is applied to fabricate ultrathin flexible or stretchable transparent conductive films, and resistive strain sensors using different polymer materials. A new wrinkle structure capacitive pressure sensor is also realized by integrating different ultrathin polymer films, and presents higher or comparable sensitivity (2.76 kPa^{-1}) compared to previous work but with a much lighter weight (<60 g m^{-2}). Wearable systems using these sensors are finally built for real time measuring wrist pulse waves, and controlling all actions of a shooting computer game with only three fingers.

1. Introduction

Flexible or soft electronics and optoelectronics, including displays, various physical, biopotential and biochemical sensors, and energy harvesters, have been developed for wearable augmented intelligence on human body in health monitoring, rehabilitation, and human–machine interaction.[1–5] To be light, soft, conformal, and thus imperceptible, these devices were fabricated on ultrathin polymer supporting films. For diverse device applications, choices of the supporting film materials need to accommodate different requirements in terms of mechanical properties (e.g., Young's modulus, elasticity), biomedical compliance, optical transparency, and cost.[6,7] Direct lamination of very thin plastic foil (e.g., polyethylene terephthalate (PET)) on a rigid carrier substrate is a popularly used method for fabrication of such devices,[8,9] but the available types of plastic foils are limited and it is also challenging to achieve tight contact free of bubbles over the whole large area. The other way to form the thin supporting layers is through vacuum evaporation (e.g., parylene)[10,11] or solution coating, followed by a delamination process.[12–14] The solution coating based approach without needing vacuum equipment is more preferred for its scalability towards large area production, and adaptability to utilizing different polymer materials. However, to obtain uniform films, the solution needs to have proper wetting properties on the carrier substrate surface for the coating process, while during lamination, the adhesion strength between the formed film and the carrier substrate must be minimized.[12] Currently, for flexible display manufacturing, laser is used to assist delamination of formed polyimide film from the glass carrier substrate by reducing the adhesion, which, however, requires high cost equipment and maintaining.[15,16] Several facile approaches using soluble separation layer were also developed, but were limited to one certain polymer material, used harmful solvent, or needed long dissolving time when using high molecular weight polymer materials to achieve low tensile stress delamination.[17–21] It would be ideal to develop a generic and scalable approach being applicable to various polymer materials for processing ultrathin soft electronics with more design and integration flexibility.

Dr. S. Chen, S. Peng, Prof. X. Guo
Department of Electronic Engineering
School of Electronics Information and Electrical Engineering
Shanghai Jiao Tong University
Shanghai 200240, China
E-mail: x.guo@sjtu.edu.cn
W. Sun, Prof. Q. Zhang
Shanghai Key Laboratory of Electrical Insulation and Thermal Aging
Department of Polymer Science and Engineering
School of Chemistry and Chemical Engineering
Shanghai Jiao Tong University
Shanghai 200240, China
E-mail: qz14@sjtu.edu.cn
Prof. G. Gu
Soft Robotics and Biodesign Lab
Robotics Institute
School of Mechanical Engineering
Shanghai Jiao Tong University
Shanghai 200240, China
The ORCID identification number(s) for the author(s) of this article can be found under https://doi.org/10.1002/admt.201800681.

DOI: 10.1002/admt.201800681

In this work, a solution based delamination process is developed using sodium hydroxide (NaOH) treated cross-linked polymethylmethacrylate (c-PMMA) film as the separation layer. The c-PMMA layer has resistance to various solvents for coating different polymer materials on top. With water permeation into the separation layer from the edge, reaction of the c-PMMA surface with the mixture of NaOH and water causes weak adhesion between the coated polymer film and the carrier substrate. As a result, the polymer film is able to be easily delaminated from the carrier substrate at near-zero tensile stress with facile processes. The approach is shown to be applicable for polymer materials of different mechanical properties, such as PMMA, polydimethylsiloxane (PDMS), poly(vinyl cinnamate) (PVC), and cross-linked polyvinyl-alcohol (c-PVA). Further, ultrathin flexible and stretchable transparent conductive films, and resistive strain sensors of low tensile force are fabricated using this approach. A new wrinkle structure capacitive pressure sensor is also developed by integrating different ultrathin polymer films, and presents higher or comparable sensitivity performance compared to previous work but with a much lighter weight less than 60 g m^{-2}. With high sensitivity and fast response, the capacitive pressure sensor is demonstrated for measuring the details of wrist pulse waves. Finally, a multisensor system composed of the resistive strain sensor and the capacitive pressure sensor is developed to control all the actions of a shooting computer game with only three fingers, proving potential for human–machine interaction applications.

2. Results and Discussion

2.1. Delamination Process

Figure 1a illustrates the developed approach for processing ultrathin polymer films using sodium hydroxide (NaOH) treated c-PMMA film as the separation layer. A mixture of PMMA and BBP-4 cross-linker with a ratio of 10:1 by weight was dissolved in propylene glycol methyl ether acetate (PGMEA) with a concentration of 60 mg mL^{-1}.[22] The solution was spin coated on the oxygen plasma treated clean glass substrate at 3000 rpm for 40 s, followed by irradiation for 15 min using a 365 nm wavelength UV light source with the power of 6000 mW cm^{-2} for crosslinking, and annealing at 150 °C for 1 h to form the c-PMMA film. After oxygen plasma treatment for 10 min to modify the c-PMMA surface,[23] a NaOH solution with a concentration of 5 mg mL^{-1} in deionization water was spin coated onto the c-PMMA film and annealed at 100 °C for 10 min. Various polymer dielectric materials, including PMMA, PDMS, PVC, and c-PVA, can then be coated on top of the separation layer. For the PMMA case, a PMMA solution at a concentration of 150 mg mL^{-1} in PGMEA was spin coated at 500 rpm for 40 s and then 1000 rpm for 40 s, followed by an annealing process at 150 °C for 1 h. For PDMS, a 10:1 mixture of PDMS elastomer (Sylgard 184, Dow Corning) to cross-linker was prepared and spin coated on NaOH layer at 4000 rpm for 40 s, followed by an annealing process at 100 °C for 10 min. To obtain conductive films, as depicted in Figure S1 in the Supporting Information, before depositing the polymer layer, silver nanowire (AgNW) suspension (Nanjing XFNANO) with a concentration of 1 mg mL^{-1} in ethanol was spin coated twice on the NaOH layer at 600 rpm for 40 s, and annealed at 150 °C for 20 min.

After the sample being immersed in deionization water for a certain time, the formed thin polymer film was delaminated from the glass substrate as shown in Figure 1b. One side of the film was attached on a metal bar using adhesive tape, and the film was able to be delaminated from the glass substrate by rolling the metal bar. With water permeation into the separation layer from the edge, the c-PMMA surface was

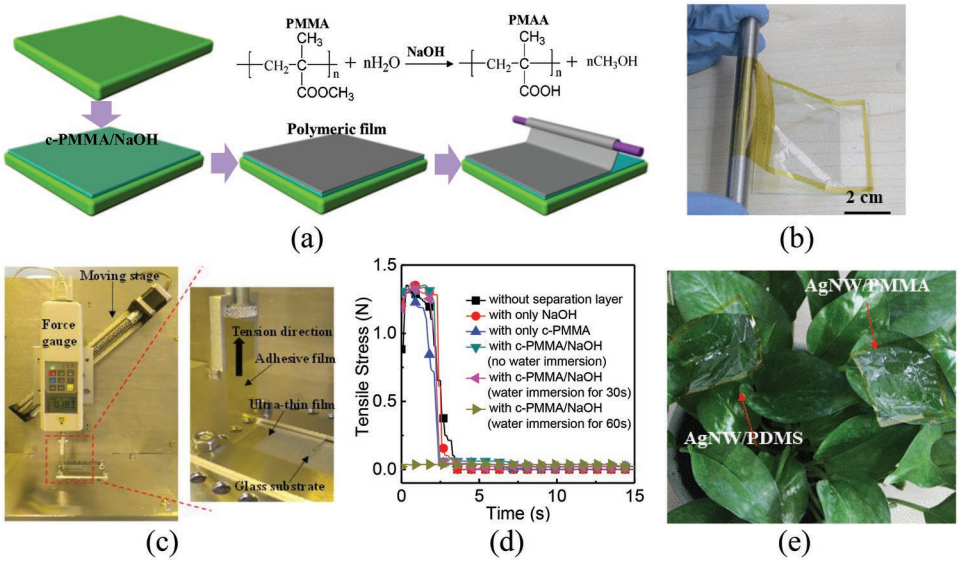

Figure 1. a) Illustration of the developed approach for processing ultrathin polymer films using water dissolvable sodium hydroxide (NaOH) on a cross-linked polymethylmethacrylate (c-PMMA) film as the separation layer. b) Photo of delamination of the thin polymer film from the glass substrate using a metal bar as the roller. c) Experimental setup for measuring the real-time tensile stress during the delamination process. d) Comparison of the measured real-time tensile stress during the delamination process for the different samples. e) The fabricated AgNW/PDMS and AgNW/PMMA films (5 cm × 5 cm) on leaves, showing their transparency and lightness.

hydrolyzed with NaOH aqueous solution through a reaction as given in Figure 1a to form hydrophilic PMAA.[24] The atomic force microscopy (AFM) images of the surface of the c-PMMA films after being soaked in the NaOH solution for different time in Figure S2 in the Supporting Information clearly show the change of the surface roughness, which further confirmed happening of the reaction. This reaction reduces the adhesion between the polymer film and the substrate surface, thus enabling a delamination process at a very low tensile stress.

To find the optimal time for immersion in water, three PDMS samples based on the proposed separation layer structure were delaminated without immersion in water, and after immersion in water for 30 and 60 s, respectively. Samples without using a separation layer, and using only c-PMMA or NaOH as the separation layer were also fabricated for comparison. An experimental setup in Figure 1c was designed to measure the real-time tensile stress during the delamination process. Figure 1d compares the measured results of the different samples. After immersion in water for 60 s, the sample using the NaOH/c-PMMA separation layer presented a very low tensile stress of about 0.04 N during the delamination process, so that the above film can be easily delaminated without damage (Figure S3a, Supporting Information). For other samples without using a separation layer, or using only c-PMMA or NaOH as the separation layer, even after immersion in water for 2 min, there was still a tensile stress of about 1.3 N. Delamination processes under such stress caused break of the films, as shown in Figure S3b,c in the Supporting Information. The measured sudden reduction of the tensile stress for these samples as shown in Figure 1d is also due to break of the films. The same approach was applied for fabricating other polymer films, including PMMA, PVC, and c-PVA with immersion in water for 2 min before lamination. As shown in Figure S4 in the Supporting Information, based on the separation layer, all films during delamination exhibit very low tensile stress, proving the generality of this approach.

With the process mentioned above, about 2.4 µm thick AgNW/PMMA and about 24 µm thick AgNW/PDMS conductive films of 5 cm × 5 cm size were obtained. The films being placed on leaves were demonstrated with excellent transparency and very light weight (Figure 1e).

2.2. Properties of the Ultrathin Conductive Films

The fabricated AgNW/PMMA film presents much higher transparency than that of commercial indium tin oxide (ITO)/PET films as seen in **Figure 2**a, especially in the short wavelength

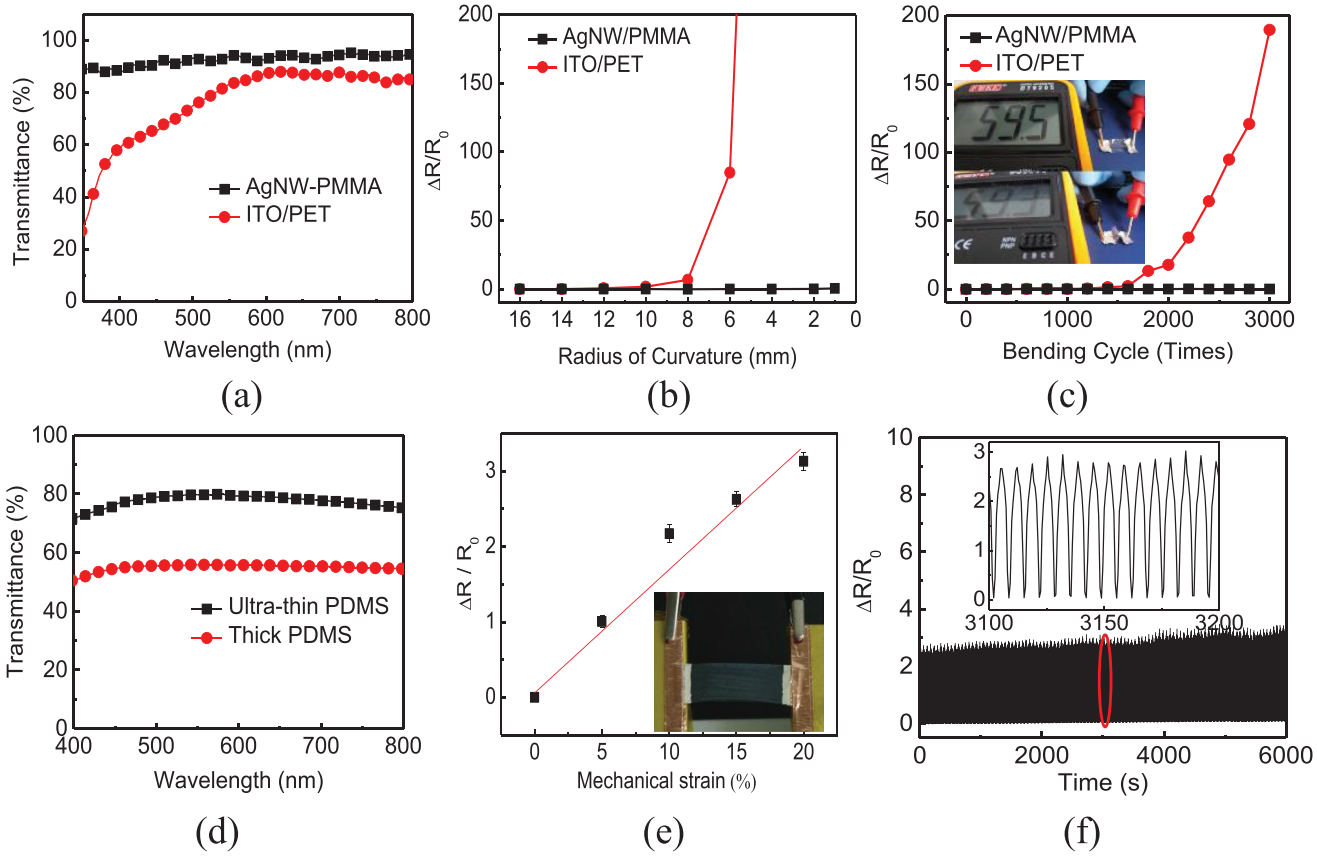

Figure 2. a) Comparison of the transparency of the fabricated AgNW-PMMA film with that of a commercial ITO/PET film. b) Measured relative resistance changes ($\Delta R/R_0$) for the AgNW-PMMA film and a commercial ITO/PET film. c) Measured $\Delta R/R_0$ for the AgNW-PMMA film and a commercial ITO/PET film for 3000 cycles of bending at a radius of 10 mm. d) Comparison of the transparency of the fabricated AgNW-PEDOT:PSS on ultrathin (about 24 µm) PDMS film and a thick (about 800 µm) PDMS film. e) Measured $\Delta R/R_0$ for the AgNW-PEDOT:PSS/PDMS film at different mechanical strain. f) Measured $\Delta R/R_0$ over time with stretching of 20% and relaxing for 3000 times.

range (400–600 nm). With an average transmittance (T) of 92.5% and a sheet resistance (R_S) of 32.1 Ω □$^{-1}$, the AgNW/PMMA film also owns larger value of Φ_{TC} ($\Phi_{TC} = T^{10}/R_S$, a commonly used figure of merit for transparent conductive films[25]) than previously reported ultrathin conductive films[9,10,17,26–30] (Table S1, Supporting Information). Figure 2b shows that the ultrathin AgNW/PMMA film can maintain unaffected electrical conductivity at a bending radius as small as 1 mm, while for the commercial ITO/PET film, an abrupt resistance increase occurring at a bending radius of 6 mm. With a bending radius of 10 mm, the AgNW/PMMA film presents negligible resistance change after 3000 cycles of bending (Figure 2c).

For the AgNW/PDMS film, an overcoating layer of poly(3,4-ethylenedioxythiophene):poly(styrenesulfonate) (PEDOT:PSS) layer was deposited on the AgNWs to effectively suppress the protrusion of AgNWs from PDMS to increase the mechanical stability.[31] The AgNW-PEDOT:PSS/PDMS film shows no change of electrical conductivity after folding (Figure S5a, Supporting Information). Such an ultrathin film presents nearly 80% transparency over the visible light wavelength range as shown in Figure 2d. With a strain more than 20%, the film exhibits significant resistance change (Figure S5b, Supporting Information). Therefore, the relative resistance change ($\Delta R/R_0$) was measured at different mechanical strain up to 20%, as shown in Figure 2e, with a gauge factor (GF) of about 15. Compared to the thicker film (about 800 µm), the ultrathin film structure requires much lower tensile force to induce the same mechanical strain (Figure S5b, Supporting Information). After stretching of 20% and relaxing for 3000 cycles, the conductivity remains unchanged as shown in Figure 2f, indicating good reliability. With features of excellent transparency, low tensile force, high durability, and fast response, the AgNW-PEDOT:PSS/PDMS thin film would be promising for fabricating unperceivable and invisible strain sensors in wearable applications.

2.3. Ultralight Capacitive Pressure Sensor

In addition to strain sensors, pressure sensors are also popularly used in various wearable applications. A new wrinkle structure capacitive pressure sensor was designed and fabricated using the processed ultrathin PDMS, AgNW/PMMA, and AgNW-PEDOT:PSS/PDMS films, as depicted in **Figure 3**a. The AgNW/PMMA film was attached onto a prestretched PDMS film with the AgNW layer facing inward. Then the PDMS film was released to its initial status, forming wrinkle structures with the AgNW/PMMA film. The AgNW-PEDOT:PSS/PDMS film was then placed on top with the AgNW-PEDOT:PSS layer facing inward to form the capacitive structure pressure sensor. In Figure 3b, the top-view photoimage of the fabricated sensor device clearly presents the wrinkle structure. With the wrinkle structure, the dielectric layer becomes much easier to be deformed upon an applied pressure compared to bulk films.[37] The deformation induces reduction of the distance between the electrodes and also increase of effective dielectric constant of the dielectric layer, resulting in capacitance change

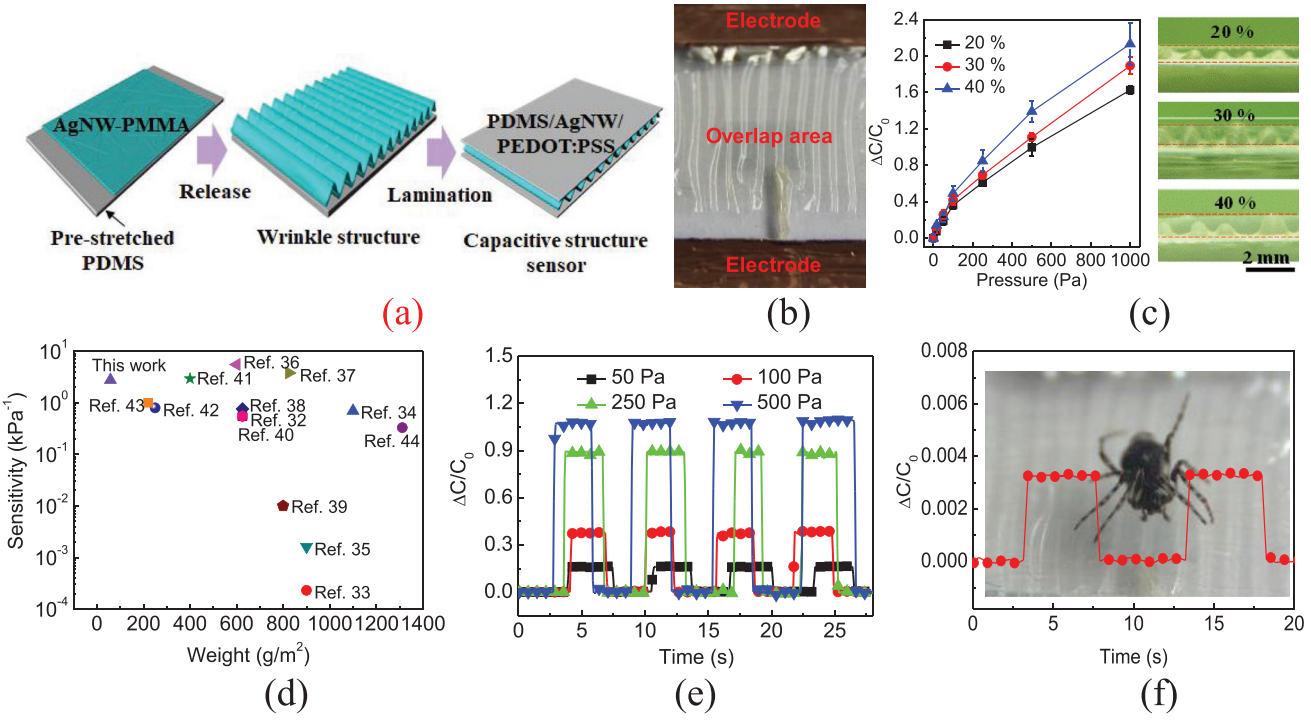

Figure 3. a) Illustration of the processes for fabricating the capacitive structure pressure sensor using the processed ultrathin PDMS, AgNW/PMMA, and AgNW-PEDOT:PSS/PDMS films. b) Top-view photoimage of the fabricated sensor device, showing the wrinkle structure. c) Measured relative capacitance changes ($\Delta C/C_0$) upon the applied pressure for the sensors fabricated with different prestretched ratios. d) Comparison of the sensitivity versus the weight of the fabricated device in this work with that of previously reported capacitive pressure sensors. e) Measured transient response of $\Delta C/C_0$ upon placement and removal of pressure of different levels. f) Measured transient response of $\Delta C/C_0$ upon a small weight of a 12 mg spider.

as measure of the applied pressure. The measured relative capacitance changes ($\Delta C/C_0$) upon the applied pressure for the sensors fabricated with different prestretched ratios and their cross-sectional photoimages are shown in Figure 3c. With a higher prestretched ratio of the PDMS substrate, the height of the wrinkle structure of AgNWs/PMMA film increased from about 0.5–1 mm. The pressure sensitivity S is defined as $S = \delta(\Delta C/C_0)/\delta P$, where C_0 is the initial capacitance of the pressure sensor and ΔC is the capacitance change with the applied pressure. The results show that higher sensitivity can be achieved with larger prestretching ratio attributed to the induced higher wrinkle structure. However, with larger prestretching ratio, the sensing performance uniformity of the fabricated devices become worse. Therefore, a prestretching ratio of 30% was used in the following studies. The fabricated sensors have a sensitivity of 2.76 kPa^{-1} at low pressure regime (0–100 Pa) and 1.56 kPa^{-1} at a higher pressure regime (100–1000 Pa). The achieved high sensitivity with such a wrinkle structure can be attributed to both the low deformation resistance of the ultrathin AgNW/PMMA film to reduce the thickness of the dielectric layer and the additional increase of the effective dielectric constant of the dielectric layer since the displaced volume under compression is air, which has a lower dielectric constant ($\varepsilon = 1.0$) than PMMA ($\varepsilon \approx 3.0$). The sensitivity versus the weight of the device is compared to that of previously reported capacitive pressure sensors in Figure 3d.[32–44] It can be seen that the sensor has higher or comparable sensitivity performance compared to previous work but with a much lighter weight less than 60 g m^{-2}. The sensor can be used to detect loads over a wide pressure range with fast response time of less than 150 ms (Figure 3e; Figure S6, Supporting Information). A small weight of a 12 mg spider is able to be detected by the pressure sensor with a thin glass slide (an area of 2 cm^2) covering the surface. This corresponds to a pressure of 0.6 Pa, indicating very low detection limit (Figure 3f). The sensor also exhibits excellent reliability by loading and unloading a pressure of 1 kPa on the sensor device for 1000 cycles (Figure S7, Supporting Information).

2.4. Wearable Applications

Attributed to the features of high sensitivity, low detection limit, and fast response, the fabricated wrinkle structure capacitive pressure sensor was used to measure the wrist pulse waves. As shown in **Figure 4**a, a simple implementation was carried out by placing the sensor on the radial artery of wrist, which was fixed

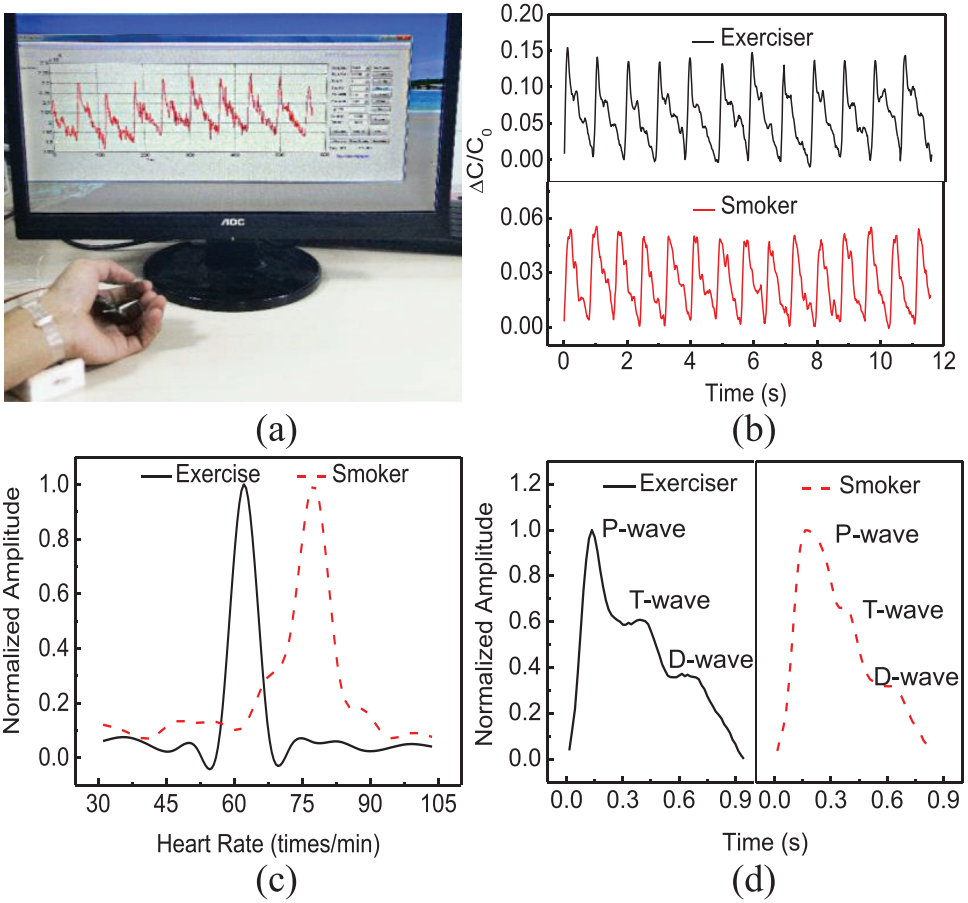

Figure 4. a) Experimental setup for measuring the wrist pulse using the fabricated pressure sensor. b) Measured real-time relative capacitance changes ($\Delta C/C_0$) over several pulse periods for two volunteers. c) Frequency domain results obtained by fast Fourier transformation (FFT) showing clear difference in the wrist pulse frequency for two volunteers. d) Results of one-period wrist pulse waveforms for the two volunteers showing the difference in the waveform shape.

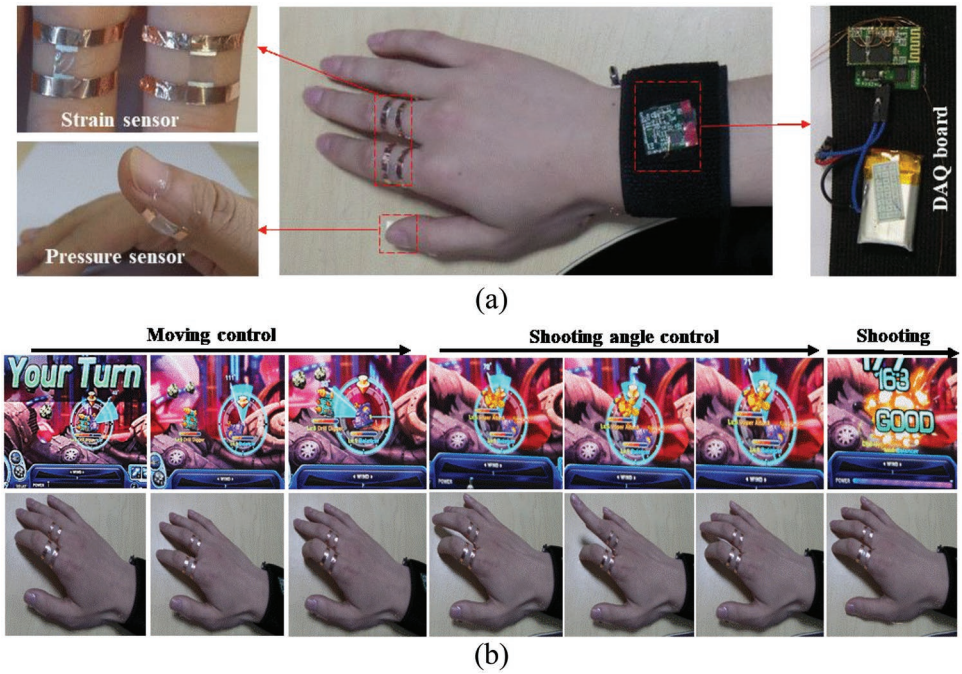

Figure 5. a) Photoimage of wearing the ultrathin strain sensors and the capacitive pressure sensors on the thumb, index and middle fingers with a data acquisition (DAQ) circuit board for controlling a small shooting game. b) Video snapshots of playing the game with only three fingers to control all the actions.

by a transparent adhesive tape. The sensor was connected to a self-designed data acquisition (DAQ) circuit board powered by a 3.3 V Li-ion battery, as depicted in Figure S8 in the Supporting Information. A software developed in MATLAB was run in the computer to process and display the data on the screen, as shown in Figure 4a. Figure 4b shows recorded real-time relative capacitance changes over several pulse periods for two volunteers. One volunteer has regular exercise (denoted as "exerciser"), and the other one often smokes (denoted as "smoker"). The measured wrist pulse frequencies for two volunteers are obviously different (≈60 beats min^{-1} for the exerciser and ≈75 beats min^{-1} for the smoker). As shown by the frequency domain results obtained by fast Fourier transformation (FFT) in Figure 4c, the frequency locations of the peaks of the waveforms are consistent with the counted numbers of beats per minute described above. One-period wrist pulse waveforms were compared in Figure 4d to show the difference in the waveform shape. The smoker has wider frequency range and stronger the percussion wave (P-wave) than that for the exerciser. The wider frequency range of wrist pulse reflects a more irregular heart rhythm, which is associated with abnormal initiation of a wave of cardiac excitation, abnormal propagation of a wave of cardiac excitation, or some combination of the two.[45] The stronger P-wave indicates that the smoker has a faster and greater momentum of blood ejection compared to that of the exerciser. Both abnormal phenomena can be contributed to the nicotine of cigarettes, which acts as an adrenergic agonist, enhances local and systemic catecholamine release, and may also stimulate vasopressin release.[46,47] The above results demonstrate that the subtle differences in wrist pulses can be identified with the pressure sensor, indicating its capability for wearable health monitoring.

To further verify the sensors for human–machine interaction applications, the ultrathin strain sensors and the capacitive pressure sensors were worn on the thumb, index and middle fingers for controlling a small shooting game as shown in **Figure 5**a. The strain sensors measuring finger bending were used to control the shooting direction and angle. The pressure sensor measuring tapping were used to trigger the fire. All the sensors were connected to the designed DAQ circuit board, which have both capacitive and resistive sensor interfaces, to collect data and transmit to the computer through the Bluetooth. The schematic of the circuit board is described in Figure S7 in the Supporting Information. Figure 5b shows the video snapshots of playing the game with only three fingers to control all the actions. The tank in the game was controlled to move to the right position by bending the index finger, and then the shooting angle was adjusted by bending the middle finger. The shooting was triggered by pressing the capacitive pressure sensor on the thumb. This simple application demonstrates the potential of integration these sensors to form a wearable system for human–machine interaction.

3. Conclusion

The developed solution based delamination approach using NaOH treated cross-linked PMMA film as the separation layer is proved to be applicable for various polymer dielectric materials, including PMMA, PDMS, PVC, and c-PVA. By using different supporting films obtained with this approach, ultrathin flexible and stretchable transparent conductive films, and resistive strain sensors are fabricated. A new wrinkle structure

capacitive pressure sensor is also developed by integrating different ultrathin polymer films, and presents higher or comparable sensitivity compared to previous work but with much lighter weight. With high sensitivity and fast response, the capacitive pressure sensor is demonstrated for measuring the details of wrist pulse waves. Finally, a multisensor system composed of the resistive strain sensor and the capacitive pressure sensor is developed to control all the actions of a shooting computer game with only three fingers. These results prove the generality of this approach for processing various ultrathin soft electronics with low cost and ease of customization to enable a wide range of wearable intelligence applications.

4. Experimental Section

Fabrication of Ultrathin Transparent Conductive Film: The mixture of PMMA and BBP-4 cross-linker with a ratio of 10:1 by weight was dissolved in PGMEA with a concentration of 60 mg mL^{-1}. The solution was spin coated on the oxygen plasma treated clean glass substrate at 3000 rpm for 40 s, followed by irradiation for 15 min using a 365 nm wavelength UV light source with the power of 6000 mW cm^{-2} for the crosslinking reactions, and annealed at 150 °C for 1 h to form the c-PMMA film. The surface of c-PMMA film was treated with oxygen plasma for 10 min, and then a NaOH solution with a concentration of 5 mg mL^{-1} in deionization water was spin coated onto the c-PMMA film and annealed at 100 °C for 10 min. The AgNW suspension (Nanjing XFNANO) with a concentration of 1 mg mL^{-1} in ethanol was spin coated twice on the NaOH layer at 600 rpm for 40 s, and annealed at 150 °C for 20 min. The PMMA, PDMS, PVC, or c-PVA solution was spin coated on the AgNW film, respectively. The PMMA (Sigma Aldrich) solution with a concentration of 150 mg mL^{-1} in PGMEA was spin coated at 500 rpm for 40 s and 1000 rpm for 40 s, followed by annealing at 150 °C for 1 h. A 10:1 mixture of PDMS elastomer (Sylgard 184, Dow Corning) to cross-linker was prepared and spin coated at 4000 rpm for 40 s, and annealed at 100 °C for 10 min. The PVC (Sigma Aldrich) solution with a concentration of 150 mg mL^{-1} in chlorobenzene was spin coated at 500 rpm for 40 s and 1000 rpm for 40 s, followed by annealing at 150 °C for 1 h. The PVA (Sigma Aldrich) and ammonium dichromate (Sigma Aldrich) as a cross-linking agent were mixed in deionized water (100 mg mL^{-1}) at a mass ratio of 6:1, and then spin coated at 3000 rpm for 40 s, followed by a crosslinking process through ultraviolet exposure (wavelength of 365 nm) for 15 min and then annealed at 100 °C for 1 h. The films were immersed in the deionization water to separate the conductive films from the glass substrate. For the AgNW/PDMS film, a PEDOT:PSS layer was deposited by spin coating to increase the mechanical stability. The AgNW/PDMS film was transferred to the clean glass, and the neutral-pH PEDOT:PSS (Shanghai OE) was spin coated on the plasma treated AgNW-PDMS film at 1500 rpm for 40 s, then annealed at 100 °C for 30 min.

Fabrication of Capacitive Pressure Sensors: The lightweight capacitive pressure sensor was fabricated using the obtained ultrathin flexible and stretchable films. The AgNW-PMMA film was attached on the prestretched ultrathin PDMS film with the AgNW film facing inward, and then the PDMS film was released to its initial length to create the wrinkle structure of the AgNW-PMMA film. The AgNW-PEDOT:PSS/PDMS film was covered on the AgNW-PMMA film with the AgNW-PEDOT:PSS to facing inward to form the capacitive pressure sensor.

Characterization: The tensile stress of the delamination process of the ultrathin films was measured by a force gauge (HP-20, Handpi). Specular transmission (T) spectra were obtained using a UV/VIS/NIR spectrophotometer (UV-3100 PC, MAPADA). The sheet resistance (R_s) was measured using a 4-point probe system (ST-2258A, Suzhou JG). The surface roughness and topography were analyzed using an AFM (Nanonavi E-Sweep, Seiko). Capacitances of the flexible pressure sensors were measured by a WK6500B impedance analyzer with a 10 kHz, 1 V amplitude AC signal. Informed consent of the participant (Sai Peng) involved in the sensor experiments had been obtained. Ethical Committee approval was not required for this study.

Supporting Information

Supporting Information is available from the Wiley Online Library or from the author.

Acknowledgements

This work was supported by the Science and Technology Commission of Shanghai Municipality (No. 16JC1400603) and the National Natural Science Foundation of China (No. 61704105).

Conflict of Interest

The authors declare no conflict of interest.

Keywords

pressure sensor, silver nanowire, strain sensor, ultrathin conductive films, wearable electronics

Received: December 5, 2018
Revised: March 11, 2019
Published online: April 12, 2019

[1] T. Yokota, P. Zalar, M. Kaltenbrunner, H. Jinno, N. Matsuhisa, H. Kitanosako, Y. Tachibana, W. Yukita, M. Koizumi, T. Someya, *Sci. Adv.* **2016**, *2*, e1501856.
[2] T. Sekitani, T. Yokota, K. Kuribara, M. Kaltenbrunner, T. Fukushima, Y. Inoue, M. Sekino, T. Isoyama, Y. Abe, H. Onodera, T. Someya, *Nat. Commun.* **2016**, *7*, 11425.
[3] Z. Zhu, R. Li, T. Pan, *Adv. Mater.* **2018**, *30*, 1705122.
[4] Q. Hua, J. Sun, H. Liu, R. Bao, R. Yu, J. Zhai, C. Pan, Z. L. Wang, *Nat. Commun.* **2018**, *9*, 244.
[5] R. A. Nawrocki, H. Jin, S. Lee, T. Yokota, M. Sekino, T. Someya, *Adv. Funct. Mater.* **2018**, *28*, 1803279.
[6] J.-H. Kim, S.-R. Kim, H.-J. Kil, Y.-C. Kim, J.-W. Park, *Nano Lett.* **2018**, *18*, 4531.
[7] Z. Lei, Q. Wang, S. Sun, W. Zhu, P. Wu, *Adv. Mater.* **2017**, *29*, 1700321.
[8] M. Kaltenbrunner, M. S. White, E. D. Głowacki, T. Sekitani, T Someya, N. S. Sariciftci, S. Bauer, *Nat. Commun.* **2012**, *3*, 770.
[9] M. S. White, M. Kaltenbrunner, E. D. Głowacki, K. Gutnichenko, G. Kettlgruber, I. Graz, S. Aazou, C. Ulbricht, D. A. M. Egbe, M. C. Miron, Z. Major, M. C. Scharber, T. Sekitani, T. Someya, S. Bauer, N. S. Sariciftci, *Nat. Photonics* **2013**, *7*, 811.
[10] K. Fukuda, Y. Takeda, Y. Yoshimura, R. Shiwaku, L. T. Tran, T. Sekine, M. Mizukami, D. Kumaki, S. Tokito, *Nat. Commun.* **2014**, *5*, 4147.
[11] J. Jean, A. Wang, V. Bulović, *Org. Electron.* **2016**, *31*, 120.
[12] C. Wang, J.-C. Chien, K. Takei, T. Takahashi, J. Nah, A. M. Niknejad, A. Javey, *Nano Lett.* **2012**, *12*, 1527.
[13] T. F. O'Connor, A. V. Zaretski, S. Savagatrup, A. D. Printz, C. D. Wilkes, M. I. Diaz, E. J. Sawyer, D. J. Lipomi, *Sol. Energy Mater. Sol. Cells* **2016**, *144*, 438.

[14] L. Zhang, H. Wang, Y. Zhao, Y. Guo, W. Hu, G. Yu, Y. Liu, *Adv. Mater.* **2013**, *25*, 5455.
[15] H. Yamaguchi, T. Ueda, K. Miura, N. Saito, S. Nakano, T. Sakano, K. Sugi, I. Amemiya, M. Hiramatsu, A. Ishida, *SID Int. Symp. Dig. Tech. Pap.* **2012**, *43*, 1002.
[16] S. Shi, D. Wang, J. Yang, W. Zhou, Y. Li, T. Sun, K. Nagayama, *SID Int. Symp. Dig. Tech. Pap.* **2014**, *45*, 330.
[17] K.-H. Ok, J. Kim, S.-R. Park, Y. Kim, C.-J. Lee, S.-J. Hong, M.-G. Kwak, N. Kim, C. J. Han, J.-W. Kim, *Sci. Rep.* **2015**, *5*, 9464.
[18] G. A. Salvatore, N. Münzenrieder, T. Kinkeldei, L. Petti, C. Zysset, I. Strebel, L. Büthe, G. Tröster, *Nat. Commun.* **2014**, *5*, 2982.
[19] R. A. Nawrocki, N. Matsuhisa, T. Yokota, T. Someya, *Adv. Electron. Mater.* **2016**, *2*, 1500452.
[20] S. Wang, J. Xu, W. Wang, G.-J. N. Wang, R. Rastak, F. Molina-Lopez, J. W. Chung, S. Niu, V. R. Feig, J. Lopez, T. Lei, S.-K. Kwon, Y. Kim, A. M. Foudeh, A. Ehrlich, A. Gasperini, Y. Yun, B. Murmann, J. B.-H. Tok, Z. Bao, *Nature* **2018**, *555*, 83.
[21] D.-H. Kim, J. Viventi, J. J. Amsden, J. Xiao, L. Vigeland, Y.-S. Kim, J. A. Blanco, B. Panilaitis, E. S. Frechette, D. Contreras, D. L. Kaplan, F. G. Omenetto, Y. Huang, K.-C. Hwang, M. R. Zakin, B. Litt, J. A. Rogers, *Nat. Mater.* **2010**, *9*, 511.
[22] Y. Liu, J. Zhao, W. Sun, Y. Huang, S. Chen, X. Guo, Q. Zhang, *Chin. J. Polym. Sci.* **2018**, *36*, 918.
[23] A. Vesel, M. Mozetic, *Vacuum* **2012**, *86*, 634.
[24] L. Zhao, H. Liu, F. Wang, L. Zeng, *J. Mater. Chem. A* **2014**, *2*, 7065.
[25] D. Y. Choi, H. W. Kang, H. J. Sung, S. S. Kim, *Nanoscale* **2013**, *5*, 977.
[26] Y. Liu, N. Qi, T. Song, M. Jia, Z. Xia, Z. Yuan, W. Yuan, K.-Q. Zhang, B. Sun, *ACS Appl. Mater. Interfaces* **2014**, *6*, 20670.
[27] D. S. Ghosh, T. L. Chen, V. Mkhitaryan, V. Pruneri, *ACS Appl. Mater. Interfaces* **2014**, *6*, 20943.
[28] Z. Liu, K. Parvez, R. Li, R. Dong, X. Feng, K. Müllen, *Adv. Mater.* **2015**, *27*, 669.
[29] C.-H. Song, C. J. Han, B.-K. Ju, J.-W. Kim, *ACS Appl. Mater. Interfaces* **2016**, *8*, 480.
[30] C. J. Han, B.-G. Park, M. S. Oh, S.-B. Jung, J.-W. Kim, *J. Mater. Chem. C* **2017**, *5*, 9986.
[31] J.-Y. Lee, D. Shin, J. Park, *Thin Solid Films* **2016**, *608*, 34.
[32] S. C. B. Mannsfeld, B. C.-K. Tee, R. M. Stoltenberg, C. V. H.-H. Chen, S. Barman, B. V. O. Muir, A. N. Sokolov, C. Reese, Z. Bao, *Nat. Mater.* **2010**, *9*, 859.
[33] D. J. Lipomi, M. Vosgueritchian, B. C.-K. Tee, S. L. Hellstrom, J. A. Lee, C. H. Fox, Z. Bao, *Nat. Nanotechnol.* **2011**, *6*, 788.
[34] J.-Y. Sun, C. Keplinger, G. M. Whitesides, Z. Suo, *Adv. Mater.* **2014**, *26*, 7608.
[35] S. Yao, Y. Zhu, *Nanoscale* **2014**, *6*, 2345.
[36] J. Wang, J. Jiu, M. Nogi, T. Sugahara, S, Nagao, H. Koga, P. He, K. Suganuma, *Nanoscale* **2015**, *7*, 2926.
[37] Y. Joo, J. Byun, N. Seong, J. Ha, H. Kim, S. Kim, T. Kim, H. Im, D. Kim, Y. Hong, *Nanoscale* **2015**, *7*, 6208.
[38] C. M. Boutry, A. Nguyen, Q. O. Lawal, A. Chortos, S. Rondeau-Gagné, Z. Bao, *Adv. Mater.* **2015**, *27*, 6954.
[39] A. P. Gerratt, H. O. Michaud, S. P. Lacour, *Adv. Funct. Mater.* **2015**, *25*, 2287.
[40] C. Pang, J. H. Koo, A. Nguyen, J. M. Caves, M.-G. Kim, A. Chortos, K. Kim, P. J. Wang, J. B.-H. Tok, Z. Bao, *Adv. Mater.* **2015**, *27*, 634.
[41] X. Shuai, P. Zhu, W. Zeng, Y. Hu, X. Liang, Y. Zhang, R. Sun, C.-P. Wong, *ACS Appl. Mater. Interfaces* **2017**, *9*, 26314.
[42] S. Wan, H. Bi, Y. Zhou, X. Xie, S. Su, K. Yin, L. Sun, *Carbon* **2017**, *114*, 209.
[43] H. Kim, G. Kim, T. Kim, S. Lee, D. Kang, M.-S. Hwang, Y. Chae, S. Kang, H. Lee, H.-G. Park, W. Shim, *Small* **2018**, *14*, 1703432.
[44] Z. He, W. Chen, B. Liang, C. Liu, L. Yang, D. Lu, Z. Mo, H. Zhu, Z. Tang, X. Gui, *ACS Appl. Mater. Interfaces* **2018**, *10*, 12816.
[45] F. H Fenton, E. M. Cherry, L. Glass, *Scholarpedia* **2008**, *3*, 1665.
[46] S. A. Al-Safi, *Eur. J. Cardiovasc. Nurs.* **2005**, *4*, 286.
[47] A. D'Alessandro, I. Boeckelmann, M. Hammwhöner, A. Goette, *Eur. J. Prev. Cardiol.* **2012**, *19*, 297.